



A computational method for rapid orthographic photography of lake sediment cores

Martin James Ankor · Jonathan James Tyler

Received: 27 January 2021 / Accepted: 17 March 2022 / Published online: 7 April 2022
© The Author(s) 2022

Abstract Photographs of sediment cores are an important dataset, often containing visual evidence for environmental change via sediment composition and structure. These photographs may be used to stratigraphically correlate adjacent cores or for automated image analysis, and can facilitate collaboration amongst researchers through sharing and annotation of the image files. Here we describe the use of computational photogrammetry (also known as Structure from Motion–Multi-View Stereo) to generate orthographic imagery of sediment cores. Computational photogrammetry is a rapid and economical technique, typically requiring only a few minutes for each metre of core, using consumer-grade digital camera equipment. The photogrammetric methodology corrects for topographic distortion caused by sediment surfaces that are not perfectly flat, and can also record features of the scene surrounding the core, such as notes, colour reference cards and measurement tapes or rulers. As the photogrammetric process also generates a three-dimensional reconstruction of the sediment core, spatial-based analysis can be used to identify damaged or non-representative sections of the core

that are to be avoided during image analysis. Using an intermittently laminated sediment core from Lake Surprise, Australia, we tested 22 scenarios using control points in a variety of configurations, as well as calibrated and uncalibrated cameras, to identify techniques that can reconstruct the core accurately and generate orthophotos. Multiple techniques were able to achieve suitable accuracy. In particular, targets placed on the table alongside the core, combined with a calibrated camera, achieved high accuracy and enabled a simple, rapid, and repeatable method for generating high-quality sediment core images.

Keywords Sediment · Core · Photography · Photogrammetry · Structure from motion · Orthophoto

Introduction

Sediment cores are important archives of palaeoclimate information. Alongside the numerous chemical, isotopic and biological indicators, sediments often contain valuable visual diagnostic information about changes in climate, environmental and hydrological conditions, including the presence of sediment structures such as ripples and turbidites, changes in sediment texture, colour and composition, or the occurrence of visible volcanic tephra (Francus 2004; Smith et al. 2013). Of particular interest are annual sediment layers (varves), which provide a means to date cores,

M. J. Ankor (✉) · J. J. Tyler
Department of Earth Sciences, University of Adelaide,
North Terrace, Adelaide, SA 5005, Australia
e-mail: martin.ankor@adelaide.edu.au

M. J. Ankor · J. J. Tyler
Sprigg Geobiology Centre, University of Adelaide, North
Terrace, Adelaide, SA 5005, Australia

as well as to develop high-resolution palaeoenvironmental reconstructions (Cooper 1998; Nederbragt and Thurow 2001; Petterson et al. 1999; Renberg 1981, 1986; Tiljander et al. 2002).

Lake sediment cores require significant time and effort to acquire and store. The acquisition of high-quality photographs to record the cores is therefore an important consideration, both prior to any destructive analysis, and over the usable life of the core. Core photographs are also essential for aligning multiple cores when developing a master sediment stratigraphy (Nakagawa et al. 2012; Obrochta et al. 2018; Petterson et al. 1999). High-quality core imagery is also necessary for the collection of sediment compositional data via calibration of sediment imagery against conventional analysis (Francus 2004; Nederbragt and Thurow 2001).

Several products have been developed over the years for scanning and analysing sediment cores, including the Itrax system (Croudace et al. 2006), the GEOTek Core Imaging System (www.geotek.co.uk), and the DMT Corescan 3 (www.dmt-group.com). These devices are extremely powerful, yet they are often expensive to purchase and operate, and may require significant time and logistical investment. This paper does not seek to assess or critique core scanning systems. Instead, we acknowledge that in many instances there is a need for simple sediment core photography, either to complement, or as an alternative when financial, logistical or time constraints mean that core scanning is not feasible. On the face of it, photographing sediment cores should be a relatively simple exercise and, when done properly, can provide high-quality data with value to a range of subsequent applications.

There are numerous challenges associated with photographing sediment cores. For example, wet sediment can reflect light, resulting in glare or specular highlights. Several methods have been developed to minimise this issue, such as scraping the surface of the core in parallel with the sediment layers to remove the overlying mud and water and expose fresh sediment, the use of cross polarisation, or covering the core with a thin layer of plastic (Francus 2004; Renberg 1981). The uneven nature of a cut sediment surface results in topographic distortion in photos (Fig. 1). Even in photographs that are taken directly normal to the core, low points that are not directly in the centre of the photo are displaced outwards from

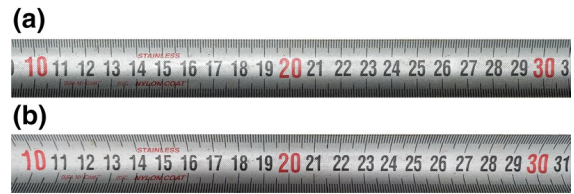


Fig. 1 An example of topographic distortion of the concave blade of a tape measure taken with **a** an 80 mm focal length (in 135 format equivalent focal length), and **b** an 18 mm focal length (in 135 format equivalent focal length)

the centre of the photo, whereas high points are displaced inwards. One technique used to minimise the effect of topographic distortion is to use just a small portion from the centre of each photograph, or a line camera (Johnson 2015; McMillan 2008). As topographic distortion increases with the distance from the centre of the photo, by using just a small portion of the centre of each photo, distortion is minimised. For example, the method suggested by McMillan (2008) uses a 1-cm-wide stripe from the centre of each photograph. This technique necessitates the use of many tens to hundreds of photos per core segment, and restricts the potential overlap available for aligning and merging photos. Requiring many photos for each core takes substantial time, and therefore intersects with another challenge encountered during core photography; sediments can react rapidly when exposed to air, and surface oxidation may take place in a matter of minutes, in addition to sediment drying, which can result in evaporite precipitation and colour change (Nakagawa et al. 2012; Renberg 1981).

We describe an alternative method, based on computational photogrammetry, also known as Structure from Motion–Multi-View Stereo (SFM-MVS). This method requires only a small number (typically 10–20) of photographs for each metre of core to rapidly generate orthographic photos of sediment cores regardless of the cut surface topography. SFM-MVS refers to the machine vision and automated software developments that have taken place over the last two decades, greatly simplifying the process of generating 3D photogrammetric models (Hossein-Nejad and Nasri 2017; Snavely et al. 2006; Westoby et al. 2012). SFM-MVS generates 3D spatial information through the identification of common points in overlapping photographs taken from different positions (Fig. 2). Once common points are identified, SFM-MVS

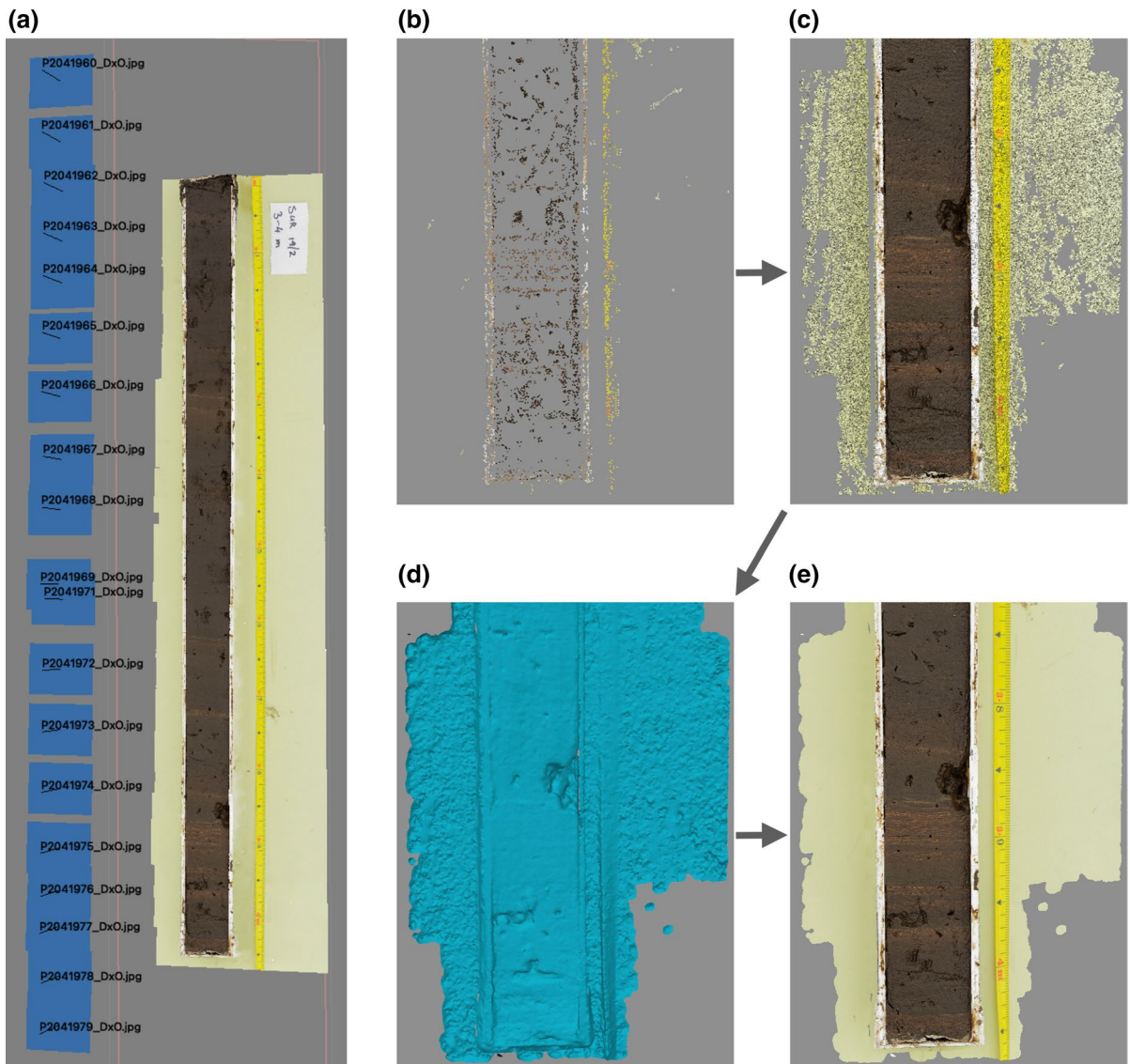


Fig. 2 **a** An overall view of the 3D reconstruction, viewed from an oblique angle. The camera positions are directly normal to (above) the exposed core surface. Each calculated camera position is represented by a blue marker square. Also

shown are images showing the photogrammetric process from **b** low-resolution point cloud, **c** high-resolution point cloud, **d** triangulated mesh, to **e** textured mesh

software calculates the camera pose for each image, as well as lens distortion, and constructs a low-resolution point cloud 3D reconstruction of the scene from the common points (Snavely et al. 2006). Once the 3D alignment stage is complete, the full photographic information is used to generate a high-resolution point cloud of the scene. The high-resolution point cloud is used to generate a solid triangulated mesh, which is then textured by the original photos. The

mesh can then be used to generate an orthographic photograph of the entire core without any topographic distortion.

Photogrammetry is most commonly used to generate digital terrain models and orthographic imagery from aerial photos. However, the technique is able to scale down to objects only a few millimetres in size and has been applied to many areas of research, including architectural, heritage, archaeological,

environmental, palaeontological, geological, geomorphological and engineering projects (Betlem et al. 2020; Citton et al. 2019; Cracknell et al. 2021; Fonstad et al. 2013; Hatzopoulos et al. 2017; Mölg and Bolch 2017; Riquelme et al. 2019; Snavely et al. 2006; To et al. 2015; Westoby et al. 2012). Jacq et al. (2021) described a method for imagery of sediment cores using SFM-MVS. We expand upon their work by quantifying the quality of 3D reconstruction and orthoimagery for 22 different SFM-MVS scenarios. Photogrammetry is an ideal tool to apply to sediment core photography as it generates a complete 3D reconstruction and orthographic image of the sediment core surface, as well as the surrounding scene, such as the table top, tape measure, notes, and colour index and white balance cards. One important benefit is that there is no need for the core to have flat surfaces, as the generation of orthoimagery removes the topographic distortion inherent within a single photo.

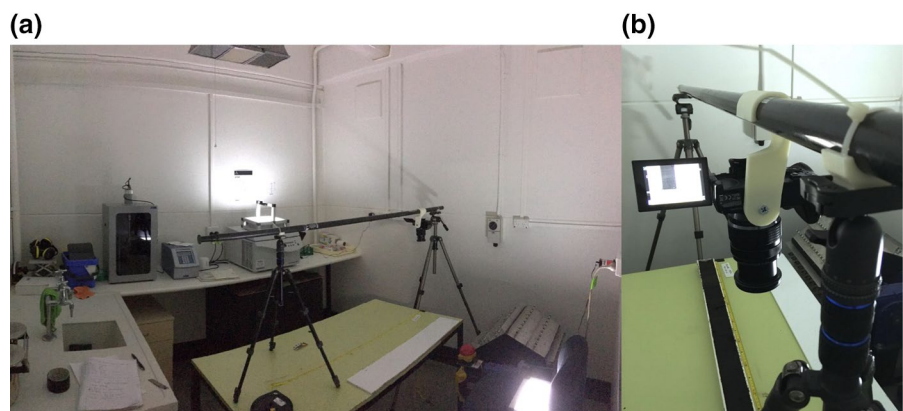
Materials and methods

The photogrammetric reconstruction of two 11-m lake cores, collected as 1-m segments, from Lake Surprise, Victoria, Australia, as well as a series of experiments investigating different SFM-MVS scenarios used similar camera rigs. For each core segment and experimental scenario the camera was mounted facing downwards on a 3D printed ‘hook’ that could slide along a 2-m pole of 30-mm diameter (Fig. 3). The pole was supported at each end by photography tripods, leaving approximately 1.5 m of free space between the tripods for the core.

Prior to setting up the rig, calculations were performed to determine the appropriate camera arrangement for a per-pixel resolution of 0.05 mm. The photography was undertaken with an Olympus E-M1 II camera, with a resolution of 5184 × 3888 pixels. For an image height of ~20 cm, this translates to a per-pixel resolution of ~0.05 mm, or ~20 pixels per mm. The pole and tripods were then set to a height that allowed for a short telephoto focal length (80 mm on 135 format), with each photo recording ~20 cm of the core. Many photogrammetry projects benefit from a wide-angle focal length (Marčič 2013), potentially because of a larger baseline between overlapping camera poses, and more robust triangulation. However, for sediment core photogrammetry, the scene is relatively simple, and usually presents little challenge for 3D reconstruction. Using normal to short telephoto focal lengths can decrease the presence of regions without data caused by obstruction by objects or topography within the scene (Hobbie 1974). Prior to beginning the core photography, test photos were taken to identify the best combination of ISO, f-stop and shutter speed. In our example, settings of f5.6, ISO400 and a shutter speed of 2.5 s produced well-exposed images with little noise and with sufficient depth of field for both the core surface, the tape measure and notes, and targets in the experimental scenarios, to be in focus.

Photogrammetry requires >60% overlap between photos. The initial and final photos were taken beyond the extents of the sediment core to ensure that the entire core was covered with overlapping photos. The camera was then moved along the pole, with a photo taken every ~7 cm, resulting in around 15 images taken per metre of core. Each metre of core

Fig. 3 **a** The lighting and room used for the Lake Surprise cores. **b** Close-up of the camera support showing the rig, camera and sliding mount



took around three minutes to photograph. If speed is required and such high resolution is not required, the image coverage may be increased, with fewer photos taken per section of core.

To minimise specular highlighting and glare, we relied on scraping the sediment to remove the thin layer of moisture exposed at the cut surface, combined with a very diffuse light source. The photography was done in a small room with white walls and ceiling. To achieve a very diffuse light, with no bright spots, upward-facing lights were bounced off the ceiling to provide a gentle light from all directions. A colour card and custom white balance were used to remove any colour cast in the photos caused by the artificial lighting. Exposure, white balance and other camera settings were kept identical for all photos. A tape measure and notes were placed alongside each core segment and recorded in the photographs. Auto-focus was used to account for any variation in camera-to-core distance.

Photographs were captured in raw format and processed using a minimal post-processing workflow consisting of minor adjustments to white balance, highlights and shadows in DXO Photolab 3 (www.dxo.com). No sharpening or edge enhancement methods were used to avoid introducing artefacts into the imagery. The effect of lens distortion on the photographs was not corrected since SFM-MVS software calculates and corrects for characteristics of lens distortion. The models commonly used for estimating lens distortion assume certain characteristics about the lens (e.g., Brown 1971) and therefore applying an additional lens distortion correction prior to SFM-MVS processing may cause problems. At the chosen focal length, the lens distortion correction was minimal, and both corrected and uncorrected images were easily processed by the SFM-MVS software. Agisoft Metashape Pro 1.7.4 (<https://www.agisoft.com>) was used for SFM-MVS processing of each sediment core segment. An accuracy setting of “High” was used for the alignment of images, dense point cloud generation and development of the mesh. Once the mesh was developed, an orthomosaic image of each core segment was generated (Fig. 4). The alignment, point cloud, mesh and orthomosaic processing is highly automated. On high settings, the processing for each core segment of 15 photos typically took less than 30 min. Many photogrammetric software packages also support batch processing, enabling

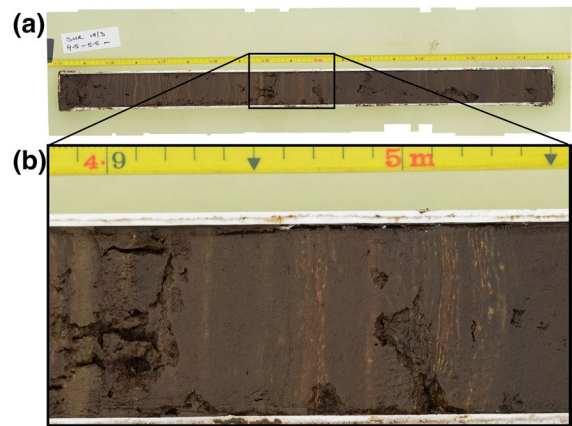


Fig. 4 **a** The full orthomosaic of 1 m of core. **b** An enlarged section showing the detail recorded

3D reconstruction and orthomosaic generation for multiple image sets unattended. Metashape Pro is a commercial product, however a similar workflow is achievable with open source software such as COLMAP (<https://demuc.de/colmap/>), or MicMac (<https://micmac.ensg.eu>).

The experimental photogrammetry scenarios used identical photographic settings and arrangement as the photogrammetry of the Lake Surprise cores, however instead of using an actual sediment core, an orthoimage of a core was printed and glued to a wooden beam (henceforth called “beamcore”) to replicate the spatial arrangement of the cores, with the beamcore surface about 40 mm above the table surface. This allowed for the experimental setup to be run over several hours with targets and check points glued or annotated directly upon the beamcore. One corner of the beamcore was twisted upwards by ~4 mm to simulate lake cores that have been cut with a slight wander or twist, and to test how vertical displacement affects horizontal errors in the 3D reconstruction.

Thirty Metashape-generated coded targets with diameters of 15 mm, similar to those described in Jacq et al. (2021), were placed in the scene (Fig. 4, Table 1). Ten were placed on the table, spaced equidistantly along each side of the beamcore (five each side). Ten more were placed at the same spacing along the outer edge of the beamcore. A further ten targets were interspersed along the edges and at the ends of the beamcore as backup/validation targets. Six check points were identified on the beamcore

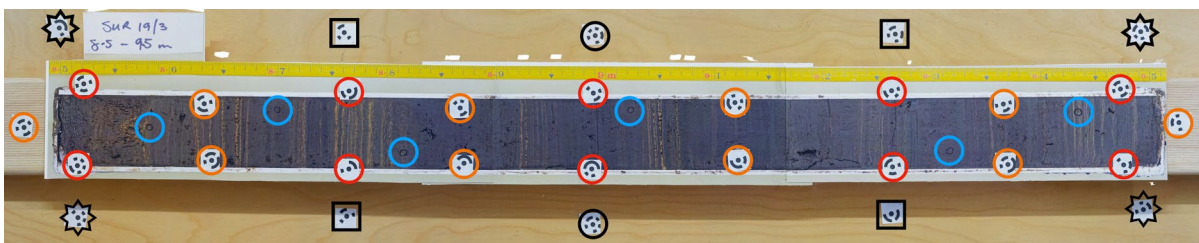
Table 1 Photogrammetry experiments showing targets used, lens parameters, and which Z values (measured or assumed as horizontal)

Recon- struction ID	Description	Lens parameters	Z Values	Targets used (Fig. 5)
A	All Targets	Derived from SFM-MVS	Measured	All
B	Table Targets	Derived from SFM-MVS	Measured	Black
C	Table Corner Targets	Derived from SFM-MVS	Measured	Black Stars
D	Table Centre Targets	Derived from SFM-MVS	Measured	Black Squares
E	Core Edge Targets	Derived from SFM-MVS	Measured	Red Circles
F	Secondary Core Edge Targets (Alternative)	Derived from SFM-MVS	Measured	Orange Circles
G	All Targets	Calibrated	Measured	All
H	Table Targets	Calibrated	Measured	Black
I	Table Corner Targets	Calibrated	Measured	Black Stars
J	Table Centre Targets	Calibrated	Measured	Black Squares
K	Core Edge Targets	Calibrated	Measured	Red Circles
L	Secondary Core Edge Targets (Alternative)	Calibrated	Measured	Orange Circles
M	All Targets	Derived from SFM-MVS	Assumed as horizontal	All
N	Table Targets	Derived from SFM-MVS	Assumed as horizontal	Black
O	Table Corner Targets	Derived from SFM-MVS	Assumed as horizontal	Black Stars
P	Table Centre Targets	Derived from SFM-MVS	Assumed as horizontal	Black Squares
Q	Core Edge Targets	Derived from SFM-MVS	Assumed as horizontal	Red Circles
R	All Targets	Calibrated	Assumed as horizontal	All
S	Table Targets	Calibrated	Assumed as horizontal	Black
T	Table Corner Targets	Calibrated	Assumed as horizontal	Black Stars
U	Table Centre Targets	Calibrated	Assumed as horizontal	Black Squares
V	Core Edge Targets	Calibrated	Assumed as horizontal	Red Circles

orthophoto. These check points were identifiable surface features such as small grains of sand, rather than targets, to better replicate the influence of sediment colour and texture on the SFM-MVS reconstruction. Targets were then located with a Leica 1203 TCRP total station and a GMP101 mini prism. Two measurements were recorded to each target and check point with the prism reinstated for each measurement. A local coordinate system was used, with X

and Y axes forming a plane approximately parallel to the table surface and the Z axis representing heights above the plane.

Twenty-two scenarios (A–V) were tested to assess a variety of target configurations, uncalibrated and calibrated camera lenses, and with Z values either measured or assumed (Fig. 5, Table 1). The aim of the experiments was to identify which photogrammetric scenarios could achieve a suitable accuracy for

**Fig. 5** Spatial arrangement for targets and check points as described in Table 1

sediment core reconstructions and orthophotography. An accuracy of 0.5 mm in the XY plane and ± 1 mm in the Z-axis was assumed as a baseline to distinguish between acceptable and inadequate results, based on what we consider would be reasonably achievable with a tape measure or rule. For a reconstruction to be considered acceptable, the interquartile range of the errors for the check points had to lie within these accuracy limits. Errors in the XY plane are clearly a concern, as they represent displacements in the reconstruction that directly affect the orthophoto. Errors in the Z axis represent displacement normal to the plane of the orthophoto. One may expect Z-axis errors to have no effect on the final orthoimage. However, an orthoimage is constructed by projecting the original photographs onto the mesh developed during the SFM-MVS process. In a perfect reconstruction with no error, the reprojected points for a specific feature of the core will align at the mesh surface. However, if the reconstructed mesh has incorrect Z values, then projected lines defining a point from two overlapping cameras will intersect above or below the mesh surface, resulting in two possible point positions and potentially resulting in blur or displacements in the orthographic photograph. Therefore, errors in the Z-axis remain a concern, both for their effect on the 3D reconstruction, as well as the potential for blur or horizontal displacement in the orthoimage.

Reconstructions C, D, I, J, O, P, T and U, which used just the corner or centre targets were designed to assess how robust the SFM-MVS process is when poorly constrained. Reconstructions E, F, K, L, Q and V, used targets placed along the edge of the beamcore. Reconstructions B, C, D, H, I, J, N, O, P, S, T, and U were performed because that spatial arrangement, with the targets placed directly on the table, represents one of the most straightforward methods to establish spatial control in two dimensions without access to precision measurement tools.

Whereas we were able to measure the Z-values (heights) of the control points to sub-millimetre accuracy, this is not a capability found in most labs, and many researchers will need to assume Z values. For the reconstructions with Z values assumed, the table targets used a single Z value based on the average of all 10 table targets. Likewise, the core edge targets used a single Z value based on the average of core edge Z values. The method used to determine the calibrated lens parameters was Agisoft Metashape's

inbuilt checkerboard pattern and lens calibration procedure. Reconstructions that used an uncalibrated camera lens derived the lens distortion parameters as part of the SFM-MVS process.

Results

The 3 dimensional coordinates of each target and check point were measured using a Leica TCRP 1203 total station and GMP101 mini prism to provide robust control and validation of the SFM-MVS reconstruction. The average positional variation for all targets and check points in the XY plane was 0.2 mm ($\sigma=0.13$ mm). The average vertical (Z) variation for all targets and check points was 0.1 mm ($\sigma=0.13$ mm).

Reconstructions A and G (Fig. 6), using all 30 targets and with lens calibrations derived from the SFM-MVS process or precalibrated using the lens calibration routine in Agisoft Metashape were expected to represent the upper limit of accuracy that can be achieved on the beamcore reconstructions. Reconstruction A achieved an average XY error of 0.08 mm ($\sigma=0.13$ mm) and an average Z error of -0.19 mm ($\sigma=0.27$ mm) for the six check points. Reconstruction G used a precalibrated camera, resulting in an average XY error of 0.17 mm ($\sigma=0.16$ mm) and an average Z error of -0.17 mm ($\sigma=0.26$ mm).

Reconstructions B, C and D all had an interquartile range (IQR) greater than the baseline. Reconstruction B, using just the table targets, had an average XY error of 0.32 mm ($\sigma=0.14$ mm), but an average Z error of 2.19 mm ($\sigma=0.34$ mm). Assessment of the unused core edge targets showed that the entire core surface had a reconstruction error in the Z-axis similar to the error found in the check points. Reconstructions C and D had low-quality results, with a curved or domed 3D reconstruction. This is a common issue when working with near-parallel photography and occurs when the SFM process fails to estimate accurately the lens distortion parameters (James and Robson 2014). The average positional errors for reconstructions C and D were 0.38 mm ($\sigma=0.24$ mm) and 0.65 mm ($\sigma=0.37$ mm), respectively, with an average vertical error of -3.4 mm ($\sigma=1.74$ mm) and 0.99 mm ($\sigma=1.84$ mm), respectively. Reconstruction E, using the targets on the core edge, had a very accurate reconstruction, with the second lowest average

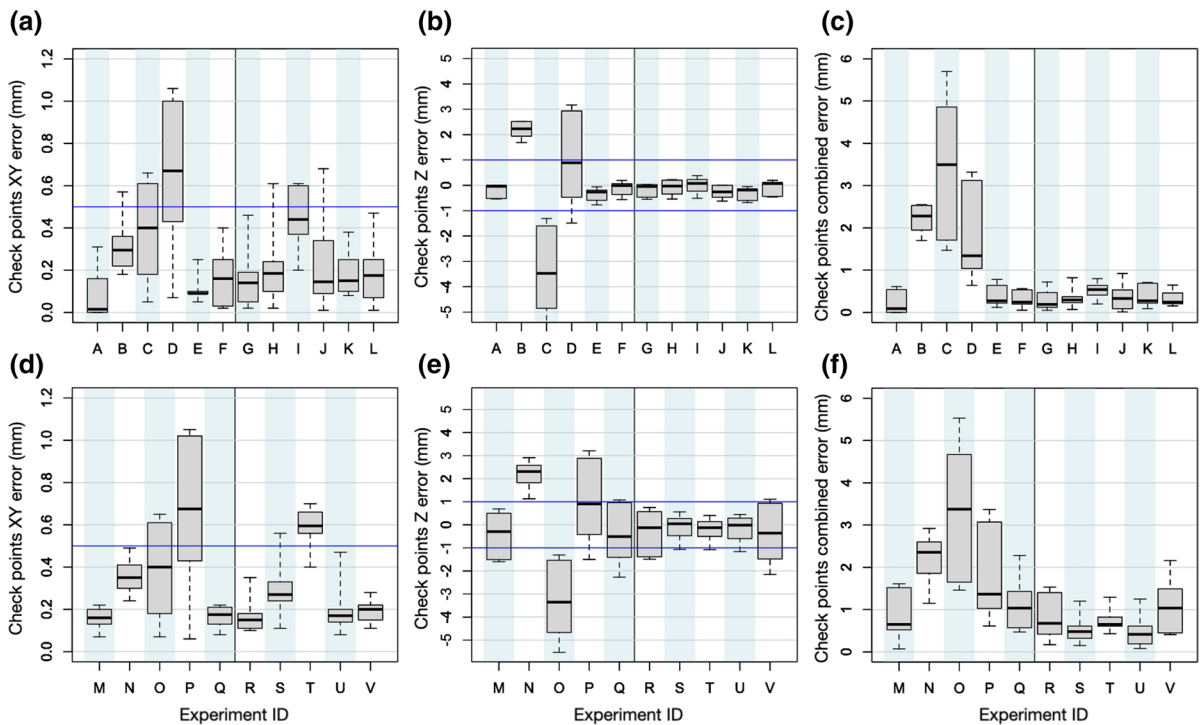


Fig. 6 **a, b, c** XY, Z and combined errors for reconstructions that used measured Z values for targets. **d, e, f** XY, Z and combined errors for reconstructions that assumed Z values for targets. For each graph, reconstructions that used estimated camera calibrations derived during the SFM-MVS process are to

the left of the black dividing line. Reconstructions that used a calibrated camera are to the right of the black dividing line. Selected accuracy limits of 0.5 mm for XY and 1 mm for Z are shown in blue

XY error of 0.11 mm ($\sigma=0.07$ mm) and a Z error of -0.36 mm ($\sigma=0.27$ mm). A second reconstruction (F), using the secondary edge targets, was performed to confirm the XY results of reconstruction E, and showed variation more in line with the other reconstructions, with an average XY error of 0.17 mm ($\sigma=0.14$ mm) and an average Z error of -0.11 mm ($\sigma=0.28$ mm).

Reconstructions G–L used the same target configurations as reconstructions A–F, combined with a calibrated camera. Using a calibrated camera gave more accurate results for all reconstructions using the table targets. Reconstructions I and J showed none of the curved reconstruction seen in reconstructions C and D. Reconstruction H, using all table targets, achieved an XY average error of 0.23 mm ($\sigma=0.21$ mm) and an average Z error of -0.09 mm ($\sigma=0.31$ mm). Reconstruction I, using just the table corner targets, failed to achieve sufficient accuracy, with an IQR extending beyond 0.5 mm in XY, XY errors of

0.44 mm ($\sigma=0.16$ mm) and a Z error of 0.00 mm ($\sigma=0.33$ mm). Reconstruction J, using the central targets on the table, had an average XY error of 0.23 mm ($\sigma=0.24$ mm) and -0.27 mm ($\sigma=0.14$ mm) for Z. Reconstructions K and L, using the targets on the edge of the core, had average XY errors of 0.18 mm ($\sigma=0.11$ mm) and 0.19 mm ($\sigma=0.16$ mm), with average Z errors of -0.31 mm ($\sigma=0.14$ mm) and -0.08 mm ($\sigma=0.29$ mm), respectively.

Reconstructions M–V used assumed Z values for targets. Reconstruction M achieved an average XY accuracy of 0.16 mm ($\sigma=0.05$ mm) and -0.42 mm ($\sigma=0.98$ mm) for Z, however the Z error IQR extended past the baseline accuracy, showing that a sizeable portion of the reconstruction did not achieve the desired accuracy. A very similar result was achieved for reconstruction R, using the precalibrated camera. Reconstructions N, O, and P, using the table targets, all failed to meet the accuracy baseline and had similar results to their equivalent reconstructions

that used measured Z values (B, C & D). The curved 3D reconstructions seen in reconstructions C and D also occurred in reconstructions O and P. Reconstruction Q, using the targets on the edge of the core, achieved a very high XY accuracy of 0.16 mm ($\sigma=0.06$ mm), though not as accurate as reconstruction E. However, as per reconstruction M, the accuracy of the reconstruction was outside the baseline accuracy for the Z-axis for portions of the core, with a Z error of -0.45 mm ($\sigma=1.31$ mm).

Reconstruction S, using all table targets, achieved an average XY error of 0.3 mm ($\sigma=0.15$ mm), with an average Z error of -0.1 ($\sigma=0.59$ mm). Likewise, reconstruction U, using just the central targets, also achieved a better than baseline average XY error of 0.2 ($\sigma=0.14$ mm) and an average Z error of -0.17 ($\sigma=0.60$ mm). However, reconstruction T, using the corner targets, did not meet the XY accuracy requirements, with an average error of 0.59 mm ($\sigma=0.10$ mm) and an average Z error of -0.22 mm ($\sigma=0.52$ mm). Reconstruction V, using the core edge targets achieved a very good XY accuracy, with an average error of 0.20 mm ($\sigma=0.06$ mm), but failed to achieve the accuracy baseline, with an average Z error of -0.38 mm ($\sigma=1.29$ mm).

The core photography of the Lake Surprise cores did not use targets. Instead, a calibrated camera was used, with a tape alongside the core to provide scale. A comparison of reconstructed lengths for 180 sections, each measuring 100 mm along the tape, resulted in standard deviation of 0.33 mm, with a maximum value of 101.10 mm and a minimum value of 99.11 mm across all 20 of the 1-m lake core segments.

Discussion

Photogrammetry offers a degree of flexibility compared to most other core photography techniques. There is no requirement for precise camera positioning, or for carefully engineered track or slider-mounted camera carriers. The main requirements are that the camera can be repositioned reasonably quickly, without disturbing the core or other components of the scene, and remain still during each exposure to avoid motion blur. If the shutter speed can be set fast enough under bright, but diffuse lighting conditions, e.g., outside on an overcast day, handheld

photography can be performed. However, in most circumstances, photography will be performed indoors, and when combined with the requirement for diffuse lighting to prevent glare and specular reflections, the camera will usually need to be stabilised.

In contrast to systems that move a core past a stationary camera (McMillan 2008), this technique does not require any editing of photos to remove background features. If the core moves relative to the background and camera, then it is necessary to remove the non-changing features in the background as they conflict with the changing features in the core as it is moved past the camera, and can confuse the automatic point identification process in SFM-MVS software. Using a photogrammetric method and a moving camera means that everything in the scene – the core, tape measure, notes, tabletop – is recorded together and used in the generation of the 3D reconstruction. The only requirement is that nothing in the scene is moved during the photography process. As photogrammetry relies on identifying common points shared across multiple photos, this also means that there is no need to have a featureless background for the core to sit upon. In fact, a textured or patterned table surface is likely to improve results, as the photogrammetric process will be able to identify and align more common points. An additional benefit to including the background as a component of the scene is that colour charts, or other optical references, may be placed alongside the entire length of the core, enabling correction for any variations in lighting.

Reconstructions using the beamcore tested different target configurations, lens calibration methods, and assumed or measured Z values. Suitable methods were identified by comparison against a baseline accuracy, based on an estimate of accuracy that could be achieved using manual measurement techniques such as tapes and rulers over a typical core length (0.5 mm in XY, and 1 mm in Z). The lens calibration appears to have the greatest influence on the quality of 3D reconstruction. Considering reconstructions A-L, all reconstructions using a calibrated lens (G-L), with the exception of reconstruction I, which used just the corner targets, achieved suitable accuracy in both XY and Z, even with sparse and poorly constrained targets. In contrast, reconstructions A-F, using an estimate of lens distortion calculated as part of the SFM-MVS process, only achieved sufficient accuracy when there was plentiful control (reconstruction A),

or when control was arrayed along the edge of the core (reconstructions E, F). This was most evident in reconstructions C and D, which had a domed or curved shape caused by incorrect SFM-MVS-derived calibration of lens distortion.

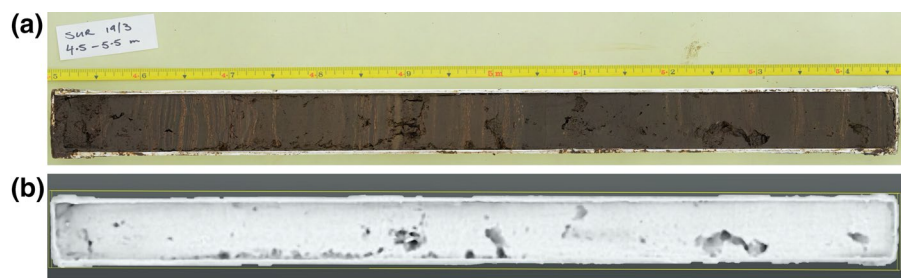
Reconstructions M–V, using assumed Z values, highlight the need for accurate vertical control. Reconstructions M–Q, using SFM-MVS-derived camera calibrations, did not achieve suitable accuracy in any scenario, with all scenarios featuring an IQR for the Z axis error greater than the baseline. Likewise, reconstructions R and V, though using a calibrated camera, and all targets or the core edge targets, did not achieve the accuracy baseline, with IQR ranges for the Z errors greater than the baseline. Only reconstructions S and U, using all table targets or the central table targets, achieved the baseline accuracy in both XY and Z. This variation in Z was expected, as the beamcore had an intentional twist with varying Z heights across the surface to simulate lake cores that have not been cut accurately and the effect of targets with incorrect Z-values. In regions where the assumed Z-values differed significantly from the measured values of the targets, the reconstruction was distorted to minimise the target error.

We therefore suggest several requirements for applying SFM-MVS to generate sediment core orthophotos. Calibration of the lens distortion parameters, using a tool like Metashape's inbuilt calibration routine, appears most important and can resolve many issues, such as the tendency to generate domed or curved 3D reconstructions, or insufficient control targets. Control targets also typically improve the quality of the 3D reconstruction, with higher numbers of targets usually generating more accurate reconstructions. However, if the control targets are not established with sufficient accuracy, then they may also cause distortions in the reconstruction, as seen in reconstructions R and V. This presents a challenge to

researchers who do not have access to precision measurement tools. The results documented in this study present a solution that can provide accurate spatial control while also being simple to establish. Reconstructions H and S, using an array of targets placed on the table, combined with a calibrated camera, were able to achieve high accuracy in both XY and Z. Targets placed on a flat surface, such as a table can be coordinated in X and Y to a high degree of accuracy, using something like gridded paper or a cutting mat, while Z can typically be assumed. In the event that a core is sufficiently raised from the table that the targets lie outside the depth of field and are blurred, the targets may then be raised nearer the plane of the core surface as per Jacq et al. (2021). Care should be taken to ensure that all targets are raised the same amount, so that Z values can still be assumed or measured accurately. In short, a general user who wishes to obtain high-quality orthometric core images without access to high-end measuring equipment should follow procedure S, with targets placed alongside the core, as per the targets marked in black in Fig. 5, and use of a calibrated camera.

Beyond the simplicity and improved efficiency for core photography, a photogrammetric workflow has further potential when used in conjunction with automated image analysis. The 3D data generated during the development of the orthographic core images also contains valuable information. For example, areas of the core that have cracks, slumps, gaps or other surface damage are not likely to be a representative image sample, and may be excluded from subsequent image analyses. Whereas these areas may not be identifiable using an approach based on image analysis, they may be readily identifiable using spatially based techniques applied to the 3D mesh or point cloud (Fig. 7). Non-representative surfaces may be identified by identifying deviation from the average surface, variations in slope, or more advanced detail recovery

Fig. 7 **a** Example of a lake core with damaged areas, and **b** the application of a PCV filter (Tarini et al. 2003) within CloudCompare (www.cloudcompare.org) to the mesh model of the core to identify damaged areas



methods such as per-pixel visibility and occlusion (Tarini et al. 2003).

Conclusions

Computational photogrammetry (SFM-MVS) is a very versatile and efficient method to document sediment cores. Although the examples documented here used a sliding rig and long shutter speeds indoors, there is no requirement for any particular camera, lighting, or even a framework or rig. As long as lighting conditions are adequate and photos are of high quality, with a common white balance, exposure and focal length, then the photogrammetric approach can be used to generate orthomosaics of a wide variety of sediment cores. Experimental results that assessed different control target configurations, calibrated and SFM-MVS-derived lens distortion parameters, and with target Z values measured or assumed, demonstrated that calibration of lens distortion characteristics was critical to maintaining accuracy of the 3D reconstruction, and that the use of targets fixed in an array beside the sediment core generally improved the quality of the reconstruction, assuming their spatial position could be well-defined. Based on the scenarios tested, one simple method that could provide well-defined control without the need for precision measurement equipment, is the use of a gridded background, such as graph paper, on a table or similar flat surface. This could provide accurate horizontal control, while the vertical values could be assumed. The photography could even be performed in the field, assuming suitable diffuse lighting is present, e.g., an overcast day. The 3D data generated during the development of the orthographic images can improve efficiency when applying image analysis techniques, as non-representative sections of the core surface such as slumps, cracks and holes can be automatically identified using the spatial characteristics of the 3D reconstruction.

Supplementary material

Metashape reports, original images, and details of the control targets used in the experimental section of this paper are available at <https://doi.org/10.17632/bcf5pct6h8.1>.

Acknowledgements We thank Cameron Barr for his valuable contributions to this paper, Patricia Gadd at the Australian Nuclear Science and Technology Organisation for her knowledge and advice regarding the Itrax system, and Asika Dhar-marathna for her assistance in collecting and preparing the core for photography. We also thank John Tibby, Bernd Zolitschka, Haidee Cadd, and Theo Cadd for their efforts collecting the Lake Surprise cores which were funded by Australian Research Council Discovery Project DP190102782.

Funding Open Access funding enabled and organized by CAUL and its Member Institutions.

Open Access This article is licensed under a Creative Commons Attribution 4.0 International License, which permits use, sharing, adaptation, distribution and reproduction in any medium or format, as long as you give appropriate credit to the original author(s) and the source, provide a link to the Creative Commons licence, and indicate if changes were made. The images or other third party material in this article are included in the article's Creative Commons licence, unless indicated otherwise in a credit line to the material. If material is not included in the article's Creative Commons licence and your intended use is not permitted by statutory regulation or exceeds the permitted use, you will need to obtain permission directly from the copyright holder. To view a copy of this licence, visit <http://creativecommons.org/licenses/by/4.0/>.

References

- Betlem P, Birchall T, Ogata K, Park J, Skurtveit E, Senger K (2020) Digital drill core models: structure-from-motion as a tool for the characterisation, orientation, and digital archiving of drill core samples. *Remote Sens* 12:330
- Brown DC (1971) Close-range camera calibration. *Photogramm Eng Remote Sens* 37:855–866
- Citton P, Ronchi A, Maganuco S, Caratelli M, Nicosia U, Sacchi E, Romano M (2019) First tetrapod footprints from the Permian of Sardinia and their palaeontological and stratigraphical significance. *Geol J* 54:2084–2098
- Cooper MC (1998) The use of digital image analysis in the study of laminated sediments. *J Paleolimnol* 19:33–40
- Cracknell K, García-Bellido DC, Gehling JG, Ankor MJ, Darroch SAF, Rahman IA (2021) Pentaradial eukaryote suggests expansion of suspension feeding in White Sea-aged Ediacaran communities. *Sci Rep* 11:4121
- Croudace IW, Rindby A, Rothwell RG (2006) ITRAX: description and evaluation of a new multi-function X-ray core scanner. *Geol Soc Lond Spec Publ* 267:51–63
- Fonstad MA, Dietrich JT, Courville BC, Jensen JL, Carbonneau PE (2013) Topographic structure from motion: a new development in photogrammetric measurement. *Earth Surf Process Landforms* 38:421–430
- Francus P (2004) Image analysis, sediments and paleoenvironments. Springer Netherlands, Dordrecht
- Hatzopoulos JN, Stefanakis D, Georgopoulos A, Tapinaki S, Pantelis V, Liritzis I (2017) Use of Various Surveying Technologies to 3d Digital Mapping and Modelling of Cultural Heritage Structures for Maintenance and

- Restoration Purposes: The Tholos in Delphi, Greece. *Mediterr Archaeol Archaeom* 17
- Hobbie D (1974) Orthophoto project planning. *Photogramm Eng Remote Sens* 40:967–984
- Hossein-Nejad Z, Nasri M (2017) An adaptive image registration method based on SIFT features and RANSAC transform. *Comput Electr Eng* 62:524–537
- Jacq K, Ployon E, Rapuc W, Blanchet C, Pignol C, Coquin D, Fanget B (2021) Structure-from-motion, multi-view stereo photogrammetry applied to line-scan sediment core images. *J Paleolimnol* 66:249–260
- James MR, Robson S (2014) Mitigating systematic error in topographic models derived from UAV and ground-based image networks. *Earth Surf Process Landforms* 39:1413–1420
- Johnson BG (2015) Recommendations for a system to photograph core segments and create stitched images of complete cores. *J Paleolimnol* 53:437–444
- Marčič M (2013) Quality of 3D models generated by SFM technology. *Slovak J Civ Eng* 21:13–24
- McMillan K (2008) An inexpensive system for continuous lake core photography. *J Paleolimnol* 40:1179–1184
- Mölg N, Bolch T (2017) Structure-from-motion using historical aerial images to analyse changes in glacier surface elevation. *Remote Sens* 9:1021
- Nakagawa T, Gotanda K, Haraguchi T, Danhara T, Yonenobu H, Brauer A, Yokoyama Y, Tada R, Takemura K, Staff RA (2012) SG06, a fully continuous and varved sediment core from Lake Suigetsu, Japan: stratigraphy and potential for improving the radiocarbon calibration model and understanding of late Quaternary climate changes. *Quat Sci Rev* 36:164–176
- Nederbragt AJ, Thurow JW (2001) A 6000yr varve record of Holocene climate in Saanich Inlet, British Columbia, from digital sediment colour analysis of ODP Leg 169S cores. *Mar Geol* 174:95–110
- Obrochta S, Yokoyama Y, Yoshimoto M, Yamamoto S, Miyairi Y, Nagano G, Nakamura A, Tsunematsu K, Lamair L, Hubert-Ferrari A (2018) Mt. Fuji Holocene eruption history reconstructed from proximal lake sediments and high-density radiocarbon dating. *Quat Sci Rev* 200:395–405
- Pettersen G, Odgaard BV, Renberg I (1999) Image analysis as a method to quantify sediment components. *J Paleolimnol* 22:443–455
- Renberg I (1981) Improved methods for sampling, photographing and varve-counting of varved lake sediments. *Boreas* 10:255–258
- Renberg I (1986) Photographic demonstration of the annual nature of a varve type common in N. Swedish lake sediments. *Hydrobiologia* 140:93–95
- Riquelme A, Cano M, Tomás R, Jordá L, Pastor JL, Benavente D (2019) Digital 3D rocks: a collaborative benchmark for learning rocks recognition. *Rock Mech Rock Eng* 52:4799–4806
- Smith VC, Staff RA, Blockley SPE, Bronk Ramsey C, Nakagawa T, Mark DF, Takemura K, Danhara T (2013) Identification and correlation of visible tephras in the Lake Suigetsu SG06 sedimentary archive, Japan: chronostratigraphic markers for synchronising of east Asian/west Pacific palaeoclimatic records across the last 150 ka. *Quat Sci Rev* 67:121–137
- Snively N, Seitz SM, Szeliski R (2006) Photo tourism: exploring photo collections in 3D. *ACM Siggraph 2006 papers*, pp 835–846
- Tarini M, Cignoni P, Scopigno R (2003) Visibility based methods and assessment for detail-recovery. *IEEE Visualization, 2003 VIS 2003*. IEEE, pp 457–464
- Tiljander M, Ojala A, Saarinen T, Snowball I (2002) Documentation of the physical properties of annually laminated (varved) sediments at a sub-annual to decadal resolution for environmental interpretation. *Quat Int* 88:5–12
- To T, Nguyen D, Tran G (2015) Automated 3D architecture reconstruction from photogrammetric structure-and-motion: a case study of the One Pilla pagoda, Hanoi, Vietnam. *Int Arch Photogramm Remote Sens Spat Inf Sci* 40:1425
- Westoby MJ, Brasington J, Glasser NF, Hambrey MJ, Reynolds JM (2012) ‘Structure-from-Motion’ photogrammetry: a low-cost, effective tool for geoscience applications. *Geomorphology* 179:300–314

Publisher’s Note Springer Nature remains neutral with regard to jurisdictional claims in published maps and institutional affiliations.